

To appear in the *Astronomical Journal*

The 3D Morphology of VY Canis Majoris. I The Kinematics of the Ejecta¹

Roberta M. Humphreys, L. Andrew Helton and Terry J. Jones

Astronomy Department, University of Minnesota, Minneapolis, MN 55455

ABSTRACT

Images of the complex circumstellar nebula associated with the famous red supergiant VY CMa show evidence for multiple and asymmetric mass loss events over the past 1000 yrs. Doppler velocities of the arcs and knots in the ejecta showed that they are not only spatially distinct but also kinematically separate from the surrounding diffuse material. In this paper we describe second epoch HST/WFPC2 images to measure the transverse motions which when combined with the radial motions provide a complete picture of the kinematics of the ejecta including the total space motions and directions of the outflows. Our results show that the arcs and clumps of knots are moving at different velocities, in different directions, and at different angles relative to the plane of the sky and to the star, confirming their origin from eruptions at different times and from physically separate regions on the star. We conclude that the morphology and kinematics of the arcs and knots are consistent with a history of mass ejections not aligned with any presumed axis of symmetry. The arcs and clumps represent relatively massive outflows and ejections of gas very likely associated with large – scale convective activity and magnetic fields.

Subject headings: circumstellar matter — supergiants — stars:winds, outflows — stars:activity — stars:individual(VY CMa)

¹Based on observations with the NASA/ESA *Hubble Space Telescope* obtained at the Space Telescope Science Institute, which is operated by the Association of Universities for Research in Astronomy, Inc. under NASA contract NAS 5-26555.

1. Introduction

The extreme red supergiant and powerful infrared source and OH maser, VY Canis Majoris is one of the most luminous evolved stars known. At its distance of 1.5 kpc (Herbig 1972; Lada & Reid 1978; Marvel 1997), VY CMA’s luminosity is $\approx 4.3 \times 10^5 L_{\odot}$ (Appendix A). Its very visible asymmetric nebula, $10''$ across, combined with its high mass loss rate of $4 \times 10^{-4} M_{\odot} yr^{-1}$ (Danchi et al. 1994), makes VY CMA a special case even among the cool hypergiants that define the upper luminosity boundary in the HR Diagram (Humphreys & Davidson 1994; de Jager 1998). VY CMA is ejecting large amounts of gas and dust at a prodigious rate, and is consequently one of our most important stars for understanding the high mass loss episodes near the end of massive star evolution.

High resolution imaging with HST (FOC, Kastner & Weintraub 1998; WFPC2, Smith et al 2001) and near-IR interferometry (Monnier et al 1999) have revealed VY CMA’s complex circumstellar environment. The multi-wavelength HST/WFPC2 images of VY CMA (Smith et al) especially showed the complexity of detail in its ejecta including the prominent nebulous arc to the northwest, which is also visible in groundbased data, two bright filamentary arcs to the southwest, plus relatively bright clumps of dusty knots near the star, and numerous small arcs throughout the nebula. All of which are evidence for multiple and asymmetric mass loss episodes. The apparent random orientations of the arcs suggested that they were produced by localized ejections, not necessarily aligned with either the star’s presumed NE/SW axis (Morris & Bowers 1980; Bowers et al 1983, Richards et al 1998) or its equator. Smith et al therefore speculated that the arcs may be expanding loops caused by localized activity on the star’s ill-defined surface.

To learn more about the morphology, kinematics and origin of VY CMA’s complex ejecta, Humphreys et al (2005) obtained long-slit spectra with HIRES on the Keck 1 telescope to map the emission and absorption lines in the nebula. The four slits were placed across several structures in the nebula including the NW arc, the two outer filamentary arcs and clumps of bright knots. The Doppler motions of the reflected absorption lines and extremely strong K I emission line revealed a complex pattern of velocities in the ejecta. Smith (2004) has also described spectra of the K I emission obtained later at similar slit positions in the nebula, but published velocities for only a few positions. Humphreys et al found a strong velocity gradient across the NW arc which is expanding at $\sim 50 \text{ km s}^{-1}$ with respect to the embedded star, and is “kinematically distinct” from the surrounding nebulosity. It was apparently ejected ≈ 400 yrs ago while the two outer filamentary arcs were ejected in separate events possibly from 800 to 1000 yrs ago. Small arcs and knots closer to the star were ejected more recently. Somewhat surprisingly, the more diffuse uniformly distributed gas and dust appeared to be essentially stationary with little or no radial velocity relative to the star.

Thus VY CMa shows evidence not only for multiple and asymmetric mass loss events at different times, but also ejections that are recognizably and kinematically separate from the general flow of the diffuse material. Obviously, these results have serious implications for the origin of high mass loss events during the final stages of massive star evolution possibly involving convection and activity analogous to that in lower mass stars. However, the overall expansion of the nebula, the direction of the outflows and orientation of the arcs within the surrounding nebulosity are not known. Fortunately, VY CMa provides us with a unique opportunity to determine the three dimensional morphology of its ejecta and the geometry of the discrete structures embedded in it.

Like other reflection nebulae, VY CMa is highly polarized. Herbig (1972) measured polarization up to 70% in the nebula, but no polarimetry has been done on VY CMa since his groundbased photographic measurements. We have obtained polarimetric images with the Advanced Camera for Surveys High Resolution Camera (ACS/HRC) on the HST together with second epoch WFPC2 images to measure the transverse motions. The polarization together with the color from the images can yield information on the line of sight distribution of the nebulosity and let us determine the relative locations of the arcs and knots, while the combined radial and transverse motions will provide the total motion and direction of the outflow of the different features.

In this first paper we describe the second epoch images, our procedure for measuring the transverse motions of the arcs and knots (§2), and the resulting kinematics of the ejecta (§3). In §4 we describe the geometry of the ejecta and in the last section we discuss the high mass loss events from active regions on the star and the presence of magnetic fields in VY CMa’s ejecta. In the second paper we will present the polarimetry measurements and the resulting three dimensional morphology of this famous object.

2. The HST Observations, Data Processing and Measurement Procedure

The second epoch images of VY CMa were observed on June 13, 2005 with the Planetary Camera on the WFPC2 with a pixel scale of $0''.0455$. The images were obtained using the medium width F410M, F547M and F1042M continuum filters and the F656N narrow band H-alpha filter. The observing program, integration times etc. were identical to that described in Smith et al. The polarimetric images were made with the ACS/HRC on August 17, 2004 using the three visual polarizers (POL0V, POL60V, and POL120V) in two colors. The F550M(V) and F658N(red) filters were chosen because they are closest to those used for the WFPC2 images. A wide range of exposure times allowed us to work close to the star and to image the fainter nebulosity. All of the new images of VY CMa obtained for this program

are summarized in Table 1.

To assure consistency of the data and our proper motion measurements we reduced the 2005 images in tandem with the reprocessing of the first epoch images from March 22, 1999. Both datasets were first processed through the standard WFPC2 pipeline at STScI. The IRAF/STSDAS task DRIZ_{CR} was used to generate bad pixel masks for both static bad pixels and cosmic rays. These masks were then applied and the images combined using the DRIZZLE routine with a scale factor of 0.5 and a pixfrac of 0.8. To remove the diffraction spikes and other artifacts, the images were then deconvolved using 3 to 5 iterations of the the IRAF task LUCY utilizing synthetic TinyTim PSFs generated for each filter. The PSFs were subsampled by a factor of two yielding a scale of 0".02275/pixel. They were then smoothed using a 3x3 to 4x4 pixel (5x5 pixel for the F1042M filter) boxcar smoothing algorithm. The short and long exposures were combined separately allowing for features to be seen in both the inner and outer regions of the nebulosity in spite of the high contrast between the two. The combined short and long exposures for each filter are labeled “s” and “l”, respectively, see Table 1. The two epochs of images, the “s” and “l” combined exposures in each filter, were then rotated and aligned on the central star. Although, the centroid of the star shifts with wavelength (Kastner & Weintraub, Smith et al 2001), by aligning the images from the same filters and with the same exposure times, we avoid the wavelength dependent shift.

2.1. The Transverse Motions

The angular expansion of VY CMa’s circumstellar nebula is not known. Maser measurements (Bowers et al 1983; Richards et al 1998) suggest an expansion of 35 km s⁻¹ near the star, while the long-slit spectroscopy showed relative velocities and shifts of 50 – 60 km s⁻¹ across the arcs. Assuming the latter, for the structures we want to measure, yields an expected positional shift of 0".051 in the 6.23 yrs between the two epochs. Although this is small, the measurements are feasible with our pixel scale.

To determine the transverse motions and direction of motion of discernible features between the two epochs, we initially examined each pair of images by eye in SAOImage DS9 to determine which features could be identified at both epochs. The more prominent features were then labeled following the naming convention in Smith et al and Humphreys et al, although it was necessary to introduce some new identifications for weaker features. Multiple positions were measured in some of the larger features such as the NW arc and they are numbered accordingly. The measured positions are identified in the accompanying images in Figures 1 – 4. Some features were more easily identified and measured in some filters than others. For example, the knots close to the star are more easily viewed and

measured in the blue exposures (F410M) while the dusty knots and filaments in the far red F1042M filter have a much smoother, more amorphous appearance making it more difficult to both identify and measure features in it.

Due to the high contrast within the nebula, it was often necessary to adjust the brightness transform within DS9 to get a comparable contrast between the two epochs for each feature. Furthermore, it appeared that VY CMa had brightened somewhat between 1999 and 2005, with some parts of the nebula especially near the star apparently brightening more than the outer nebulosity, thus supporting suggestions of variable illumination (Wallerstein 1978; Monnier et al 1999). The images were then blinked between the two epochs and the x and y pixel coordinates of the peak transmission of each recognizable feature were recorded. This process was repeated for each feature in all of the combined short and long exposures in which it could be identified. Three independent measurements were made of each feature by working through the entire set of images before beginning the measurements a second and third time. The average of the net shifts in arcsec for the separate features is given in Table 2 for each filter and exposure time combination. The errors were determined from the standard deviation of the three measurements, and are likely higher than any systematic errors arising from rotation, alignment and deconvolution. Although our procedure adjusted for possible variable illumination, it may contribute to the random errors. All of the measurements are included in Table 2, however for those features measured in three or more images, we could occasionally identify discrepant measurements or positions very likely due to the complexity of the ejecta and variable appearance of some of the features in the different filters. These are identified in the footnotes to Table 2 and are not included in the mean transverse velocity weighted by the standard deviation (Table 3). When a feature was measured in two images where the positions in either epoch disagreed by more than 5 pixels, they are flagged as separate features in the footnotes.

In Table 3 we give the projected radial distance and the position angle from the star in the plane of the sky for each measured feature with its weighted mean transverse velocity (V_T), its associated error in km s^{-1} and its direction of motion (ϕ), determined from the mean angular shift in the x and y coordinates between the two epochs with the error of the mean. The vectors are shown as arrows on Figures 5 – 7 corresponding to the features marked in the Figures 1 – 4. In the next section we combine the transverse and Doppler velocities for a discussion of the kinematics of the ejecta, the motions of specific arcs and knots, their ages and orientations and the overall expansion of the nebula.

3. The Kinematics of the Ejecta

Humphreys et al obtained long-slit spectra at four positions across the nebula shown in Figs. 1a and 1b in that paper. Three parallel slit positions crossed the NW arc along the SE/NW direction and sampled clumps of knots and filaments closer to the star. The fourth, oriented roughly NE–SW, crossed the two outer filamentary arcs 1 and 2. Spectra were extracted from regularly-spaced apertures along the slits selected to cover specific features as listed in Table 2 of the 2005 paper. These data provide the Doppler velocities discussed below for positions across the nebula and specific features in the WFPC2 images.

The most complete and precise Doppler velocities in these data are provided by the K I $\lambda 7699$ emission line, which we attribute to resonance scattering at the observed locations. In principle the observed K I feature might represent any of four processes: (1) resonance scattering as just mentioned; (2) local thermal emission; (3) potassium recombination; or (4) emission or pseudo-emission produced near the star and then reflected toward us by dust grains in the observed regions. For cases 1–3 the apparent Doppler shifts have the usual meaning; but case 4 involves the “moving mirror” effect which alters the relation between space motion and net Doppler shift². Which is correct? Some relevant quantities were estimated in the first half of Appendix A in Humphreys et al. The scarcity of potassium makes cases 2 and 3 very unlikely for such a prominent feature. Possibility 4, reflection by dust, is less likely because the measured line components at most of our measured positions are sharper and less complex than those seen close to the star. Moreover, if we interpret the measured Doppler shifts in the normal way as velocities along the line of sight, then we find plausible and self-consistent results described below; but this is not true if we adopt the “moving mirror” formula instead. We therefore assume that the strong K I $\lambda 7699$ component measured at each position is caused by local resonance scattering. Strictly speaking we cannot *prove* this, but it is the simplest explanation, there is no apparent evidence against it, and it leads to reasonable conclusions³.

If the 7699 Å pseudo-emission feature observed in a condensation represents resonance scattering by K I, then one might ask whether its apparent wavelength is perturbed by K I

²Doppler velocities are available for a few strong absorption lines reflected by local dust but they involve the moving-mirror effect and are difficult to use.

³ In the second half of Appendix A in Humphreys et al, we describe a way to avoid a line-formation problem in the extremely strong K I emission line viewed *near the central star*. That problem does not arise in the material discussed in the present paper, thousands of AU from the star. For our purposes here it is sufficient to view resonance scattering as simple reflection limited to the line’s narrow velocity width in each local arc or condensation.

self-absorption along our line of sight through the surrounding material. There are several arguments against that possibility. First, the spatial extent of each measured line component almost perfectly matches the corresponding feature in the WFPC2 images; this can be seen in our 2D spectra, e.g., Figs. 9 and 12 in Humphreys et al. Second, the line component that we measured at most of the locations is rather simple, not asymmetric or multiple as would likely occur with additional self-absorption. Third, as estimated in Appendix A of the 2005 paper, the line-center optical depths are not predicted to be large except within dense condensations; potassium should be very thoroughly ionized. In summary, there is no reason to think that significant self-absorption occurs.

Obviously, with only four slits the entire nebula was not covered, and consequently only about two-thirds of the features (40 out of 66) listed in the preceding tables have Doppler or radial velocities. Our quoted values for the local line-of-sight velocity V_z are all relative to the VY CMa’s reference frame which we assume to be the K I emission Doppler velocity at the central star, $\approx +41.0 \text{ km s}^{-1}$. For reasons indicated in Humphreys et al, this may introduce an uncertainty of a few km s^{-1} but there is no evident way to determine the correction⁴. The three components of the motions for these features are summarized in Table 4. We combined our measured transverse velocity with the corresponding Doppler velocity (V_z) to determine the total space motion (V_{Tot}) and the combined direction of motion, θ . The slit and extraction aperture for the Doppler velocity from Humphreys et al are given in the comment column. In those cases where multiple velocity components are present along the line of sight, an explanation is provided as a footnote to Table 4 or in the following discussion of the kinematics of the more prominent features.

3.1. The “Nebulous” Northwest Arc

In their analysis of the Doppler velocities for both the reflected absorption lines and the K I emission, Humphreys et al reported a strong velocity gradient across the nebulous arc to the northwest of the star. The broadened absorption lines were significantly redshifted with a velocity difference of $\sim +50 \text{ km s}^{-1}$ relative to the star due to the moving mirror effect. Although the direction of the flow was not known, the evidence from the line widths, the P Cygni profiles, etc., suggested expansion velocities between 35 and 70 km s^{-1} and that the motion of the material in the arc was mostly transverse at an angle of $\pm \sim 20^\circ$ with respect to the plane of the sky.

We have measured 10 different positions along the NW arc. Combining the transverse

⁴VY CMa’s expected systemic velocity is $\sim 37 \text{ km s}^{-1}$.

velocities with the emission line velocities at the same positions we determine a mean total space motion for the arc of $45.7 \pm 4 \text{ km s}^{-1}$ at an angle θ of $22 \pm 7^\circ$ away from us along the line of sight. The results for the separate positions range from 28 to 69 km s^{-1} and θ from 7.5 to 38° . At its distance from the star and taking the mean projection angle into account, the material in the arc was ejected about 500 yrs. ago.

It is possible that radiative acceleration may have altered the r/V_{Tot} ratios used to estimate the time since the ejection. We can estimate this for the NW Arc whose mass is roughly known ($\sim 3 \times 10^{-3} M_\odot$ (Smith et al)). As seen from the star, the NW Arc covers less than 300 square degrees and therefore intercepts no more than 1% of the total luminosity. The corresponding momentum flux would accelerate this mass at about $10^{-4} \text{ cm s}^{-2}$ or $\approx 15 \text{ km s}^{-1}$ in 500 yrs. In that case, about one third of the observed outward speed may be due to post-ejection acceleration which would reduce the age estimate from 500 to 400 yrs. The real effect is most likely smaller because radiative acceleration would tend to disrupt the observed coherent structure of the arcs. Therefore, we expect the effect to be small on the estimated ages and have neglected it for the NW Arc and the other features in the ejecta.

Humphreys et al suggested that the section of the arc near the tip where it appears to be bending back toward the star, may actually be the nearer side. Unfortunately, there were no measurable knots or features in this section that were sufficiently resolved to confidently measure the motions. However, adopting our expansion velocity and the moving mirror velocity relative to the star of 40 km s^{-1} for the absorption lines at this location (Humphreys et al) we derive an angle $\sim -7.5^\circ$ out of the plane, towards us, compared to $+10^\circ$, using the same method, for the same absorption lines along the major axis of the NW arc. Thus this section of the arc does appear to be nearer.

3.2. The Outer Filamentary Arcs 1 and 2

The K I emission lines across Arcs 1 and 2 show complex profiles and multiple peaks due to flows or streams of gas identified with these two very visible arcs. (See the profiles in Figure 11 and the two-dimensional image of the slit in Figure 13 in Humphreys et al.) The extraction aperture across Arc 2 has two very prominent emission peaks. One has a large positive velocity like that of the reflected absorption lines which we also attribute to reflection by the background material, while the blueward peak, which represents a separate flow of emitting gas along the line of sight, is most likely produced by resonant scattering. We have therefore adopted this emission velocity for the radial component of the motions in Arc 2 which is -19 km s^{-1} relative to the star. A strong blueshifted emission feature which first appears weakly in aperture 5 can be traced over $3''$ and across Arc 1. This is

a kinematically separate flow of gas from that associated with Arc 2, and Humphreys et al identified this emission with resonant scattering by the gas in a flow associated with Arc 1. This gives a radial velocity relative to the star of -37 km s^{-1} .

The transverse motions for the six positions measured in Arc 2 show that they are moving in different directions (Figure 6) consistent with an overall expansion of the arc like a bubble or loop with a net motion to the south. Three of our positions correspond to the extraction aperture across Arc 2. Adopting the corresponding radial velocity described above gives a mean space motion or expansion velocity of $64 \pm 2.1 \text{ km s}^{-1}$ at an angle of -17° , towards us along the line of sight. At this angle and at a distance 3.4 arcsec from the star, the material in Arc 2 was ejected 460 yrs ago, about the same time as the NW arc.

Similarly for Arc 1, three of our measured positions with transverse motions have corresponding radial velocities and give a mean expansion velocity of $68.2 \pm 2.5 \text{ km s}^{-1}$ out of the plane of the sky towards us at an angle of -33° . The transverse motions measured at eleven different positions along the arc indicate an expansion of the loop with a net motion of the material to the SSW on the sky. At its distance from the star and moving at an angle of 33° , Arc 1 was ejected about 800 years ago.

Thus both Arcs 1 and 2 are most likely in the foreground, moving towards us, but at significantly different angles and in different directions.

3.3. The W Arc

Humphreys et al described this feature as a small irregularly shaped arc between the star and the more prominent NW arc. Our measurements show that this feature is made up of several small knots moving in an approximately northwest direction. Two separate slits cross the different knots or positions we measured for the transverse motions (Slit III ap 3 and Slit I ap 3), but like numerous places in the nebula, the K I emission line has more than one velocity component in these apertures. After inspection of the line profiles and the 2-dimensional image of Slit III in Figure 9 in Humphreys et al, we adopted the velocity peaks at 41.7 km s^{-1} for III ap 3 and 45.6 km s^{-1} for I ap 3. The latter is used only for knots D1 and D2 which based on their position may be distinct features separate from the W arc. These adopted velocities, yield essentially zero radial motion relative to the star and a total space motion of $\approx 44 \text{ km s}^{-1}$ to the northwest in the plane of the sky. The corresponding time since the ejection is $\approx 300 \text{ yrs}$.

If we had chosen the slower radial velocity feature at $\sim 25 \text{ km s}^{-1}$, the knots in the W arc would be moving towards us (-17°) at $\sim 50 \text{ km s}^{-1}$ and ejected 275 yrs ago.

3.4. The SW Knots

Several small knots can be easily discerned in the WFPC2 images of VY CMa just to the southwest of the star. Knots A, B, C and G in this grouping are in the Slit III ap 2 extraction. We adopted the K I velocity component at 27.3 km s^{-1} , yielding a radial velocity relative to the star of -14 km s^{-1} for these knots. It is not clear if this clump of knots is gravitationally bound or moving together. However, if we treat them as a group, they are apparently moving out of the plane at -25° with a net space motion of $36 \pm 5.5 \text{ km s}^{-1}$. Their net transverse motion towards -86° is essentially to the west, except for knot B. However, given the range in their vector motions, this feature could also be interpreted as a clump whose separate knots are expanding away from each other. Assuming that they were ejected together at the same time, it occurred about 250 yrs ago. If we had adopted the other velocity component, (44.5 km s^{-1}) we would have concluded that the SW knots are moving essentially in the plane of the sky, but with little change in the expansion velocity (33 km s^{-1}) or the time since their ejection.

3.5. The S knots

This group of small knots directly to the south of the star is similar in appearance to the SW group. Knots A, B, C, and Y are in Slit V ap 3 while knots D1 and D2 are in Slit III ap 2. For the latter, we adopted the same velocity component used for the SW knots, while at Slit V, one of the emission components is the same as that measured for the absorption lines and is therefore associated with reflection from the surrounding material; see discussion above for Arcs 1 and 2. The other much stronger emission peak at 37 km s^{-1} gives a velocity relative to the star of -17 km s^{-1} . The knots are thus in the foreground at an angle of -27° . The S knots are moving to the southeast, position angle $\sim 156^\circ$, except for knots D1 and D2 which given their position, may be part of a separate feature. The mean space motion or expansion velocity is $41.6 \pm 5 \text{ km s}^{-1}$. This gives a time since the ejection of only 157 yrs, the most recent age among the variety of embedded structures that we have discussed. With an uncertainty of ± 25 yrs for the mass loss episode, the S knots, and the subsequent formation of dust, may correspond to VY CMa's fading from ~ 6.5 mag to 8 mag from ~ 1870 to 1880.

3.6. The S Arc

The S Arc stretches approximately east to west about $2''.5$ to $3''.0$ from the central star. Slit V crosses knot B in the S arc between apertures V ap4 and V ap5. with three and two emission peaks in each aperture, respectively. We associate the most redshifted velocity with background material as discussed for Arc 2. This leaves K I emission features at 25 km s^{-1} and 52 km s^{-1} for possible kinematic identification with the material in the S Arc. Their respective velocities relative to the star are -16 km s^{-1} and $+11 \text{ km s}^{-1}$ corresponding to -22° and $+16^\circ$ for the S Arc's orientation with respect to the plane of the sky. We favor the foreground orientation based on the appearance of the S Arc, but either is possible. The total space velocity is $\sim 41 - 42 \text{ km s}^{-1}$, and the time since the ejection is 480 yrs in both cases.

3.7. The SE Loop

We measured transverse motions at three positions on the small SE Loop or arc on the east side of VY CMA's asymmetric ejecta. Slit III crosses knot B on the SE loop, but Humphreys et al did not include an extraction at that position which is near the end of the slit. We therefore went back to the original spectrum and measured a Doppler velocity at that position of $+17.5 \text{ km s}^{-1}$, corresponding to a velocity relative to the star of -23.5 km s^{-1} . The SE Loop is therefore in the foreground at an angle of -21° moving to the southeast. The space motion for knot B is 65.1 km s^{-1} , yielding an age of ~ 320 yrs. The SE Loop is the only feature on the east of the ejecta for with measured transverse motions. There were no easily measured knots in "arc 3" identified by Smith et al also on the east side of the nebula.

3.8. The SW Clump

What we have called the SW Clump is one of the more perplexing features in the ejecta. It is close to the star, but only seen in the far red F1042M filter and is located between the SW and S groups of knots. It is obviously very red and dusty. Two of the long slit extraction apertures overlap the SW Clump, but since this feature is totally obscured at the shorter wavelengths, it is uncertain if the measured radial velocities at this position are applicable; although, the K I emission line is in the far-red at 7700\AA . Since the SW Clump is highly obscured it seems reasonable to assume that it is not a foreground feature, so we have adopted the more redshifted velocities in these two apertures of $42 - 44 \text{ km s}^{-1}$ which gives

a negligible radial velocity with respect to the star. If this is the case, the SW clump is moving slightly away from us ($\sim +8^\circ$) quite slowly at only $\approx 18 \text{ km s}^{-1}$ to the SSW, and was ejected about 500 yrs ago.

3.9. General Expansion of the Nebula

Over much of the extended nebula, the K I emission line has a velocity component at or near its heliocentric velocity measured at the star (41.0 km s^{-1}) and the expected systemic velocity of $\sim 37 \text{ km s}^{-1}$ (Bowers et al 1983). Indeed, in the outer parts of the nebula, the K I emission line is often double, showing both of the above velocities (Tables 4 and 6 in Humphreys et al). The K I lines in the outer ejecta are also very narrow ($10 - 15 \text{ km s}^{-1}$), indicative of very little Doppler broadening. Furthermore, the $\text{H}\alpha$ line, which is quite weak on and near the star, becomes relatively strong in the outer parts of the nebula which Humphreys et al attributed to nebular emission from the nearby H II region (Sharpless 310). Its velocity agrees with the systemic velocity and with the same velocity feature in the K I emission line. Thus we also attribute the latter to reflection by dust in the surrounding medium, not to VY CMa’s ejecta. This still leaves the K I emission near 40 km s^{-1} which if due to reflection by the ejecta, implies virtually no radial expansion relative to the star. Thus any measurement of transverse motion in the diffuse nebulosity (separate from the arcs and knots) is important to determine any overall expansion of the nebula.

Unfortunately, this proved difficult due to the lack of measurable features in the more diffuse outer ejecta. We did measure the transverse motions for several “spikes” or extensions at the western edge of the visible nebulosity; some of which had quite high transverse motions (Table 3). Two of these also had measured Doppler velocities at $35 - 42 \text{ km s}^{-1}$; thus their radial motion relative to the star is $\sim 0 \text{ km s}^{-1}$ and their total space motion is nearly all transverse at $30 - 40 \text{ km s}^{-1}$. At $6''$ to $7''$ from the star this material would have been ejected about 1300 to 1700 years ago.

Humphreys et al also noted broad wings on the K I emission lines in the outermost ejecta along all four slit positions. The wings have Doppler velocities which average -136 km s^{-1} and $+208 \text{ km s}^{-1}$ at positions between $7''$ and $9''$ from the star. They very likely represent faster moving, more diffuse gas and dust perhaps from an earlier more uniform ejection or wind.

4. Discussion – Geometry of the Ejecta

The results for the spatially recognizable features discussed in the preceding section are summarized in Table 5. Except for the NW arc and perhaps the SW Clump, all of the measured features appear to be moving either close to the plane of the sky or toward us. This is not surprising, since within about $3''$ of the star, most of the diffuse nebulosity appears to be optically thick. Evidently, we do not see through the nebula and do not see many features, presumably on the other side, moving away from us. Figures 8 – 10 show 3D representations of the positions of the knots for which we have total space motions. The figures show their positions relative to the plane of the sky assuming uniform radial expansion viewed from three different perspectives ⁵. Our results for the vector motions of the major arcs and the clumps of knots clearly show that these structures were not only ejected at different times, but are also moving in different directions and at different angles relative to the plane of the sky and to the star. This is definitely suggestive of random locations for the sites of the ejection episodes on the star and the directions of the outflows.

The extensive maser (OH, H₂O, SiO), and CO observations however, have been interpreted as evidence for an axis of symmetry with possible bipolar outflows and a disk-like distribution for the circumstellar material, although, the models for the geometry of the system based on the different maser distributions and CO maps, are not always consistent with each other. Most of the maser spots and the intensity maxima are also quite close to the star, typically within $0''.5$, consequently there is little correlation with the optical knots and arcs discussed in this paper. Only our NW knot is this close to the star, but its position does not appear to correspond to any of the maser emission spots.

The OH maser intensity maxima are within $0''.5$ and are distributed along a NE-SW axis at a position angle of $\sim 50^\circ$ (Bowers et al 1983) which could be tilted 15 to 30° to our line of sight. If there is a NE-SW polar/rotation axis, then arcs 1 and 2 could both be part of an associated bipolar outflow depending on the opening angle of the cone, but from different locations on the star corresponding to the separations of their vector motions of $\sim 15^\circ$. In this case, as Humphreys et al suggested, the NW arc would then be near the corresponding equatorial plane. With this assumed geometry, the three prominent arcs could correspond to ejection episodes near the polar and equatorial axes, but the S and SW clumps and other smaller arcs would be ejected from more random directions.

The H₂O maser spots appear to be oriented much more east-west (Richards, Yates & Cohen 1998). The highly polarized SiO maser spots (Shinaga et al 2004) have a $0''.2$ north-

⁵This 3D visualization can be viewed as a movie at www.astro.umn.edu/~ahelton/research/VYCMa.

south distribution on the sky, although their polarization vectors have a mean position angle of 72° in agreement with the orientation of the bipolar axis of the SiO emission. Similarly, diffraction – limited speckle interferometry in the near – infrared also shows a primarily north-south orientation for the dust shell extended $0''.2$ with a position angle ~ 153 to 176° (Wittkowski, Langer & Weigelt 1998), while near-IR aperture-masked interferometry (Monnier et al 1999) showed a southward extension of the dust emission within $0''.1$ but no clear disklike or bipolar geometry in the images. K-band interferometric measurements however, indicate a bipolar distribution within $0''.1$ of the star but with the dusty disk oriented east-west (Monnier et al 2004). Recent interferometric millimeter observations of CO and SO (Muller et al 2006) have been modelled as a bipolar outflow in the east-west direction, but with a very wide opening angle ($\sim 120^\circ$) and an expanding shell elongated north-south.

With this lack of strong evidence for a well-defined or preferred axis of symmetry or bipolar axis in VY CMa, we conclude that the kinematics and corresponding morphology of the numerous arcs and knots are more consistent with *a history of localized mass ejections from active regions on the star not strongly aligned with a presumed axis or equator*.

VY CMa’s asymmetric circumstellar nebula, extended to the west and south of the star, is very apparent in the optical images. The more prominent embedded arcs and knots are also found to the west and south of the star, although the smaller SE loop and arc 3 (Smith et al 2001) are to the east of the star. The nebula appears much more symmetric in the infrared with more symmetric contours at $2\mu\text{m}$ and in the thermal infrared (see Figures 4 and 5 in Smith et al). Smith et al also showed that the reddening and apparent extinction was much higher to the east and north of the star. They suggested that a combination of higher extinction plus possible back-scattering, assuming a NE-SW axis of symmetry, could account for the lack of visible nebulosity to the east and northeast. This interpretation may be supported by the contours at $9.8\mu\text{m}$ which appear to be compressed or foreshortened to the northeast. We also want to point out, however, that VY CMa is on the western edge of the large dark cloud Lynds 1667 and at the same distance. Thus its asymmetric appearance could be due entirely to obscuration.

5. Conclusions – Convective Activity, Magnetic Fields and Mass Loss

We first suggested in Smith et al that the complex ejecta of arcs and knots revealed in the first epoch HST/WFPC2 images resulted from ejection episodes, possibly involving large scale convection and magnetic fields. We also demonstrated that the arcs are too massive to have to have been ejected by radiation pressure alone and that the initial ejection was caused by some other process. The measured Doppler velocities in Humphreys et al showed that

the arcs were kinematically separate from the surrounding diffuse material and represented separate gas flows expanding relative to the star. With the addition of the transverse motions reported here, ages, velocities, and directions of the outflows confirming their origin from eruptions at different times and from spatially separate regions on the star not by a more uniform long-term mass loss.

Smith et al estimated the mass of the NW arc to be $\sim 3 \times 10^{-3}M_{\odot}$ from its surface brightness in a two arcsec² section, assuming an optical depth of unity. This is likely an underestimate because the NW arc is may be optically thick. Similarly, Arcs 1 and 2 are also the visible loops or bubbles produced by large outflows of gas extending over several arc seconds on the sky (Humphreys et al), and are probably as massive as the NW arc. Assuming $3 \times 10^{-3}M_{\odot}$ in each of these three arcs plus the S and SW clumps of knots, there may be more than $\approx 1.5 \times 10^{-2}M_{\odot}$ in these features. This is $\approx 10\%$ of the total mass of $0.2 - 0.4 M_{\odot}$ (Smith et al) in the nebula, and this does not take into account the numerous small filaments and knots visible throughout the nebula or similar outflows not visible through the nebula. With a dynamical time scale of 3 yrs, the short-term mass loss rate associated with the NW arc and similar features is $\sim 10^{-3}M_{\odot} \text{ yr}^{-1}$, several times the average mass loss rate.

The expected duration for a convective event or nonradial pulsation would likely be on the same order as VY CMa’s dynamical timescale of 3 yrs or perhaps slightly longer. If each of the more prominent features, the arcs and clumps of knots represents a temporary mass loss of the order of $3 \times 10^{-3}M_{\odot}$, then the total kinetic energy in the NW arc, for example, expanding at 46 km s^{-1} is 6×10^{43} ergs. This is modest compared to the $\sim 2 \times 10^{47}$ ergs VY CMa would radiate in 3 yrs, and is also comparable to the thermal energy in the ejected mass.

In our two previous papers on VY CMa we have suggested that the expanding arcs, loops, and clumps of knots are the result of localized activity on the star related to convection and magnetic fields. Nonradial pulsational instability may be an alternative ejection mechanism, but the distinction may be vague for a red supergiant where the convective cells are expected to be comparable to the stellar radius in size (Schwarzschild 1975); although, nonradial pulsations would not be expected to produce the narrow arcs and loops observed in VY CMa. Starspots and large “asymmetries” have now been observed on several stars including red giants, AGB stars and supergiants. The best example among the red supergiants is probably α Ori (Gilliland & Dupree 1996), but stellar hotspots have also been observed on α Sco and α Her with properties consistent with a convective origin (Tuthill, Haniff & Baldwin 1997). Monnier et al (2004) have reported on high resolution imaging of evolved M stars including NML Cyg, VX Sgr and VY CMa revealing large-scale inhomogeneities and deviations from uniform brightness which they attribute to magnetic fields and/or rotation.

Recently, Vlemmings et al (2002, 2004) have estimated the magnetic field strength from the circular polarization of H₂O masers in the ejecta of AGB stars and several evolved supergiants including the strong OH/IR sources VY CMa, VX Sgr, NML Cyg, and S Per. They report magnetic fields in VY CMa of ~ 200 mG at distances of 220 AU. Their analysis supports the Zeeman interpretation of the circular polarization of the SiO masers only a few AU from the surface of the stars (Barvainis et al 1987; Kemball & Diamond 1997). Together with Zeeman splitting of the OH emission far out in the wind at a few thousand AU (Szymczak & Cohen 1997; Mashedder et al 1999), these measurements confirm the presence of a magnetic field throughout the ejecta of VY CMa. Each of these results imply magnetic fields of the order of 10^4 G at the star’s surface assuming the r^{-2} dependence of a solar-type magnetic field that would be associated with large star spots, convective activity and the mass ejections.

VY CMa is a member of a relatively small group of evolved, highly unstable, massive stars called cool hypergiants, that are just below the empirical upper luminosity boundary in the HR Diagram. Among this high luminosity group a few stars stand out, the OH/IR supergiants mentioned above plus IRC+10420, with exceptionally high mass loss rates, and resolved circumstellar ejecta (Humphreys et al 1997, 2002, Schuster, Humphreys & Marengo 2006). There is no evidence for a close companion in any of these stars which could be responsible for their mass loss and ejecta (see Smith et al for VY CMa). These stars may represent a short-lived stage with episodes of high mass loss. We are thus observing increasing evidence among the evolved massive stars (η Car, LBVs, and the cool hypergiants) for episodic mass loss. In the cool hypergiants (IRC+10420, VY CMa, VX Sgr, S Per, NML Cyg), the high mass loss episodes may be driven by large -scale convection and magnetic fields. In Paper II we present the polarimetry and the three dimensional spatial structure of VY CMa’s circumstellar ejecta.

We thank Kris Davidson for many helpful discussions and George Wallerstein for reading and commenting on a draft of the manuscript. It is always a pleasure to thank George Herbig for his support and continued interest in VY CMa. This work was supported by NASA through grant number GO10262 from the Space Telescope Science Institute.

Facilities: HST (WFPC2) HST (ACS)

A. The Luminosity of VY CMa and Its Position on the HR Diagram

The luminosity of VY CMa ($L \sim 4 - 5 \times 10^5 L_{\odot}$) is well-determined from its spectral energy distribution and distance, and places it near the empirical upper luminosity limit in

the HR Diagram for cool hypergiants. In a recent paper however, Massey, Levesque & Plez (2006) suggest that VY CMa is nearly a factor of 10 less luminous than has previously been determined by several authors. They assert that its high luminosity and other “extreme” properties such as its inferred large size were based on an adopted effective temperature that was too low (e.g. $\sim 2800^\circ$, Le Sidaner & LeBetre (1996)).

Massey et al fit recent optical spectrophotometry of VY CMa with MARCS model atmospheres and derived a much warmer effective temperature. Combining its apparent visual magnitude, an adopted interstellar extinction, and a temperature dependent bolometric correction, they derive a luminosity $L \sim 6 \times 10^4 L_\odot$ instead of the usually quoted $\sim 4 - 5 \times 10^5 L_\odot$. However, this classical approach ignores one of VY CMa’s distinguishing characteristics, its spectral energy distribution and large excess radiation in the infrared.

A recently published example of its energy distribution can be seen in Figure 7 in Smith et al. Most of the star’s radiation is reprocessed by the dust in its extensive circumstellar ejecta. Its energy distribution rises rapidly in the infrared and has a broad maximum between 5 and 10 μm . Combining the photometry in Tables 3 and 4 in Smith et al for the entire nebula with the IRAS data from 25 to 100 μm , and integrating the apparent energy distribution, yields a luminosity of $L = 4.3 \times 10^5 L_\odot$ at VY CMa’s distance of 1.5 kpc (Herbig 1972, Lada & Reid 1978, Marvel 1997, the same distance used by Massey et al.) If corrected for *interstellar* extinction at visual and red wavelengths, the luminosity would increase by only a few percent, because most of the most of the flux is escaping at $\sim 10\mu\text{m}$. Furthermore, an A_v of 3.2 mag (Massey et al) implies that at least 2 mag of more of circumstellar extinction is required in the visual to equal the flux emitted at $10\mu\text{m}$. The wavelength dependence of the CS extinction correction, however, is not known.

The standard “textbook” approach, relying only on visual photometry and spectroscopy and an assumed temperature, is not valid for stars with sufficient circumstellar dust to reradiate their visual and red flux in the thermal infrared. In some cases, the radiating dust also dominates the observed flux between 1 μm and 5 μm and contributes significant circumstellar extinction at visual, red and near-infrared wavelengths. Other well-studied examples in our galaxy are VX Sgr, S Per, and NML Cyg. Like VY CMa, all three are strong maser sources and NML Cyg is optically obscured. See Schuster, Humphreys & Marengo (2006) for recent images of these stars.

In summary, the luminosity proposed for VY CMa by Massey et al is far less than what is actually observed, and there is little doubt that it is near the empirical upper luminosity limit in the HR Diagram for the cool hypergiants (Humphreys & Davidson 1979, 1994).

Further consideration of VY CMa’s exact position on the HR Diagram depends on the

assumed surface temperature. Previously published spectral types for VY CMa in the past 30 years or so have been mostly in the M4-M5 range; although, Massey et al suggest that VY CMa’s apparent spectral type is more likely \sim M2.5 based on the MARCS model atmosphere fit to their spectrum. Interestingly, though, the blue TiO bands in their published spectrum (Figure 2 in Massey et al) are more like their M4-type reference spectrum than the M2-type spectrum they show. This author’s numerous spectra of VY CMa obtained over many years have all been in the M4-M5 range. Therefore, adopting the M4–M5 spectral type with the temperature scale proposed by Levesque, et al (2005) gives $T_{eff} \sim 3450\text{--}3535^\circ$, while an older scale (used in Humphreys & McElroy 1984 from Flower 1977) yields $T_{eff} \sim 3200^\circ$ for an M4-M5 star.

However, one should be cautious in the case of VY CMa; *we are not observing either its photosphere or its surface directly*. It has been known for some time that VY CMa’s absorption spectrum is significantly redshifted with respect to its systemic velocity (Humphreys 1975, Wallerstein 1977) due to scattering by dust (Herbig 1970, Kwok 1976, Van Blerkom & Van Blerkom 1978). Indeed, most of VY CMa’s visual-red radiation originates by reflection and scattering by the dust grains at 100 AU from the star, the dust formation radius. Only a few percent of the radiation actually escapes through the dust shell, which is very likely inhomogeneous, implying optical depths of 4 to 5 at $\sim 7000\text{\AA}$ in its wind (Humphreys et al). If the wind is opaque, then R_{ph} where the photons arise, could be larger than the true stellar radius, and the underlying star possibly somewhat warmer.

Massey et al also suggest that with previous temperature estimates, VY CMa would violate the Hayashi limit. But the cause of the apparent conflict with the Hayashi limit is the assumed temperature not the luminosity. Whether or not it violates the Hayashi limit depends on whether the adopted temperature, inferred from the strength of the TiO bands or an atmospheric model, is indicative of the star’s ill-defined surface or its wind. With the above temperatures, VY CMa is on the edge or just inside the Hayashi limit as plotted in Figure 1 in Massey et al., but the standard Hayashi limit applies to hydrostatic atmospheres. Non-spherical outflows and a resulting dense wind as in VY CMa may affect the Hayashi limit’s location on the HR Diagram.

VY CMa’s high luminosity and apparent low temperature suggest that it is one of the largest stars known. Monnier et al (2004) derived a radius of $3000 R_\odot$ from $2 \mu\text{m}$ interferometry. Given the above arguments, $3000 R_\odot$ is probably not the actual size of the imbedded star. Adopting this radius with VY CMa’s luminosity gives an “effective” temperature of $\sim 2700^\circ$ which is rather low. Alternatively, with the apparent temperatures given above, the radius is 1800 to $2100 R_\odot$. In either case, *VY CMa is obviously very luminous, cool and big*.

REFERENCES

- Barvainis, R., McIntosh, G. & Predmore, C. R. 1987, *Nature*, 329, 613
- Bowers, P. F., Johnston, K. J., & Spencer, J. H. 1983, *ApJ*, 274, 733
- Danchi, W.C., Bester, M., Degiacomi, C.G., Greenhill, L.J., & Townes, C.H. 1994, *AJ*, 107, 1469
- de Jager, C. 1998, *A&A Rev.*, 8, 145
- Flower, P. J. 1977, *A&A*, 54, 31
- Gilliland, R.L. & Dupree, A. K. 1996, *ApJ*, 463, L29
- Herbig, G.H. 1970a, *Mem. Soc. Roy. Liege*, 19, 13
- Herbig, G.H. 1972, *ApJ*, 172, 375
- Humphreys, R. M. 1975, *PASP*, 87, 433
- Humphreys, R.M. & Davidson, K. 1979, *ApJ*, 232, 409
- Humphreys, R.M. & Davidson, K. 1994, *PASP*, 106, 1025
- Humphreys, R. M., Davidson, K., Ruch, G., & Wallerstein, G. 2005, *AJ*, 129, 492
- Humphreys, R. M. & McElroy, D. B. 1984, *ApJ*, 284, 565
- Kastner, J. H. & Weintraub, D.A. 1998, *AJ*, 115, 1592
- Kemball, A. J. & Diamond, P. J. 1997, *ApJ*, 481, L111
- Kwok, S. 1976, *JRASC*, 70, 49
- Lada, C.J. & Reid, M.J. 1978, *ApJ*, 219, 95
- Le Sidaner, P. & Le Betre, T. 1996, *A&A*, 314, 896
- Levesque, E.M., Massey, P., Olsen, K. A. G., Plez, B., Josselin, E., Maeder, A., & Meynet, G. 2005, *ApJ*, 628, 973
- Marvel, K.B. 1997, *PASP*, 109, 1286
- Mashedier, M. R. W. et al 1999, *New Astronomy*, 43, 563
- Massey, P., Levesque, E. M., & Plez, B. 2006, *ApJ*, 646, 1203

- Monnier, J. D., Tuthill, P. G., Lopez, B., Cruzalebes, P., Danchi, W. C. & Haniff, C. A. 1999, *ApJ*, 512, 351
- Monnier, J. D. et al. 2004, *ApJ*, 605, 436
- Morris, M. & Bowers, P. F., 1980, *AJ*, 85, 724
- Muller, S., Dinh-V-Trung, Lim, J. Hirano, N., Muthu, C, & Kwok, S. 2006, *ApJ*, submitted
- Richards, A. M. S., Yates, J. A., & Cohen, R. J. 1998, *MNRAS*, 299, 319
- Shinnaga, H., Moran, J. M., Young, K. H. & Ho, P. T. P. 2004, *ApJ*, 616, L47
- Schuster, M. T., Humphreys, R. M., & Marengo, M 2006, *AJ*, 131, 603
- Schwarzschild, M. 1975, *ApJ*, 195, 137
- Smith, N., Humphreys, R. M., Davidson, K., Gehrz, R. D., Schuster, M. T. & Krautter, J. 2001, *AJ*, 121, 1111
- Szymczak, M. & Cohen, R. J. 1997, *MNRAS*, 288, 945
- Tuthill, P. G., Haniff, C.A. & Baldwin, J. E. 1997, *MNRAS*, 285, 529
- Van Blerkom, J. & Van Blerkom, D. 1978, *ApJ*, 225, 482
- Vlemmings, W. H. T., Diamond, P. J. & van Langevelde, H. J. 2002, *A&A*, 394, 589
- Vlemmings, W. H. T., van Langevelde, H. J., & Diamond, P. J. 2004, *Mem S. A. It.*, 75, 282
- Wallerstein, G. 1977, *ApJ*, 211, 170
- Wallerstein, G. 1978, *Observatory*, 98, 224
- Wittkowski, M., Langer, N., & Weigelt, G. 1998, *A&A*, 340, L39

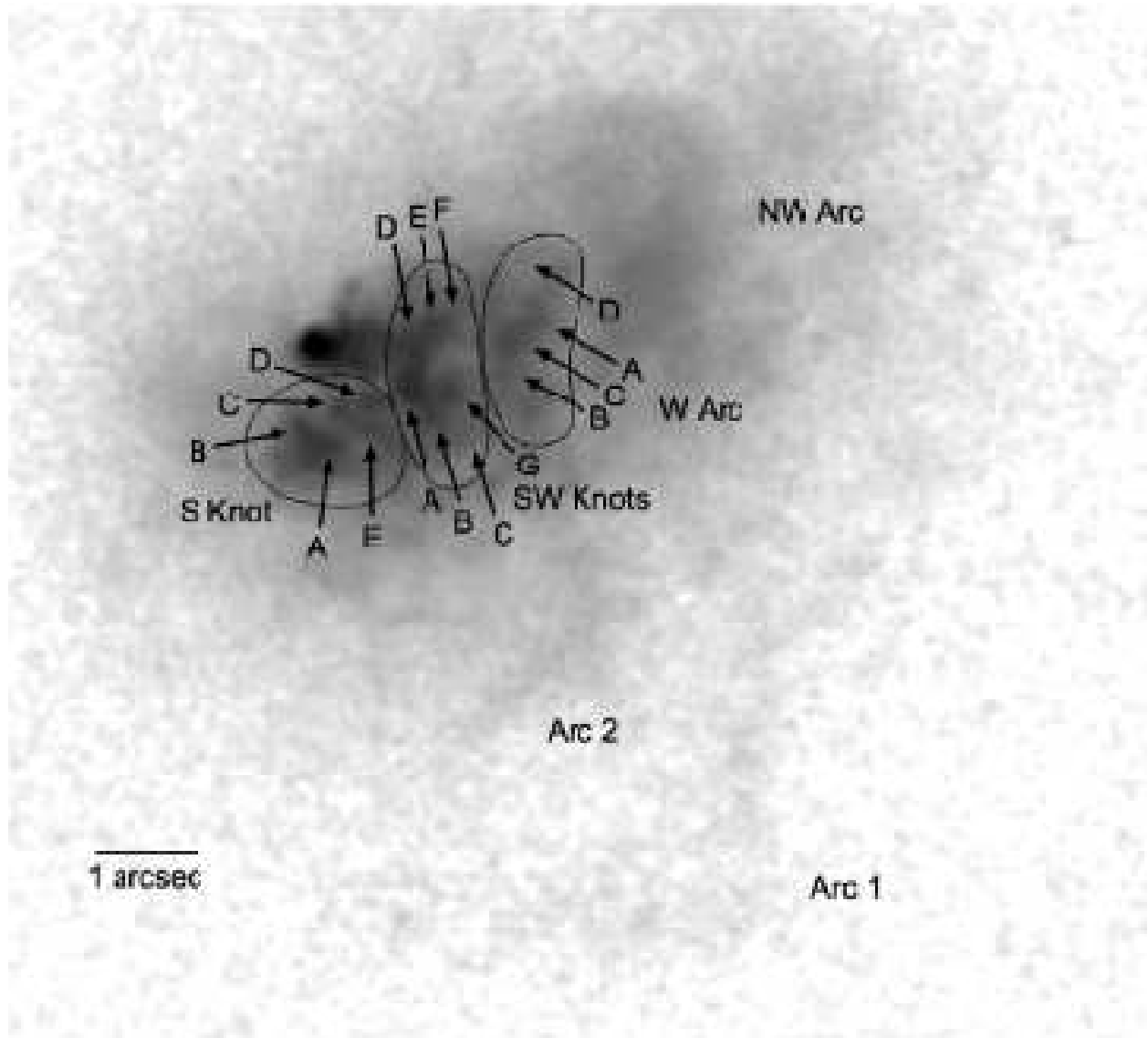


Fig. 1.— The F410M image showing the features in the inner ejecta including the S and SW knots.

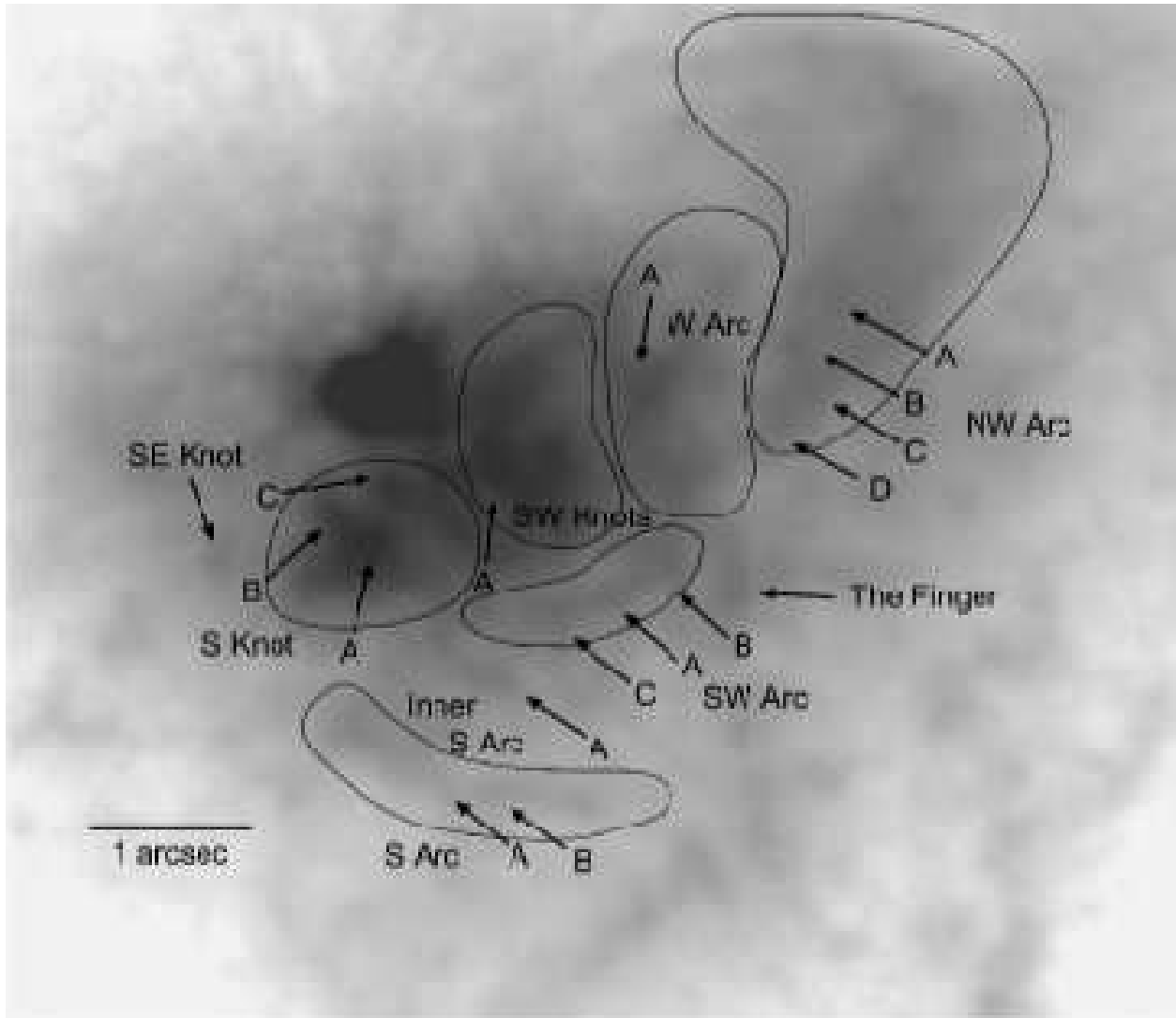


Fig. 2.— The F547M image showing measured features in the ejecta including positions in the NW arc.

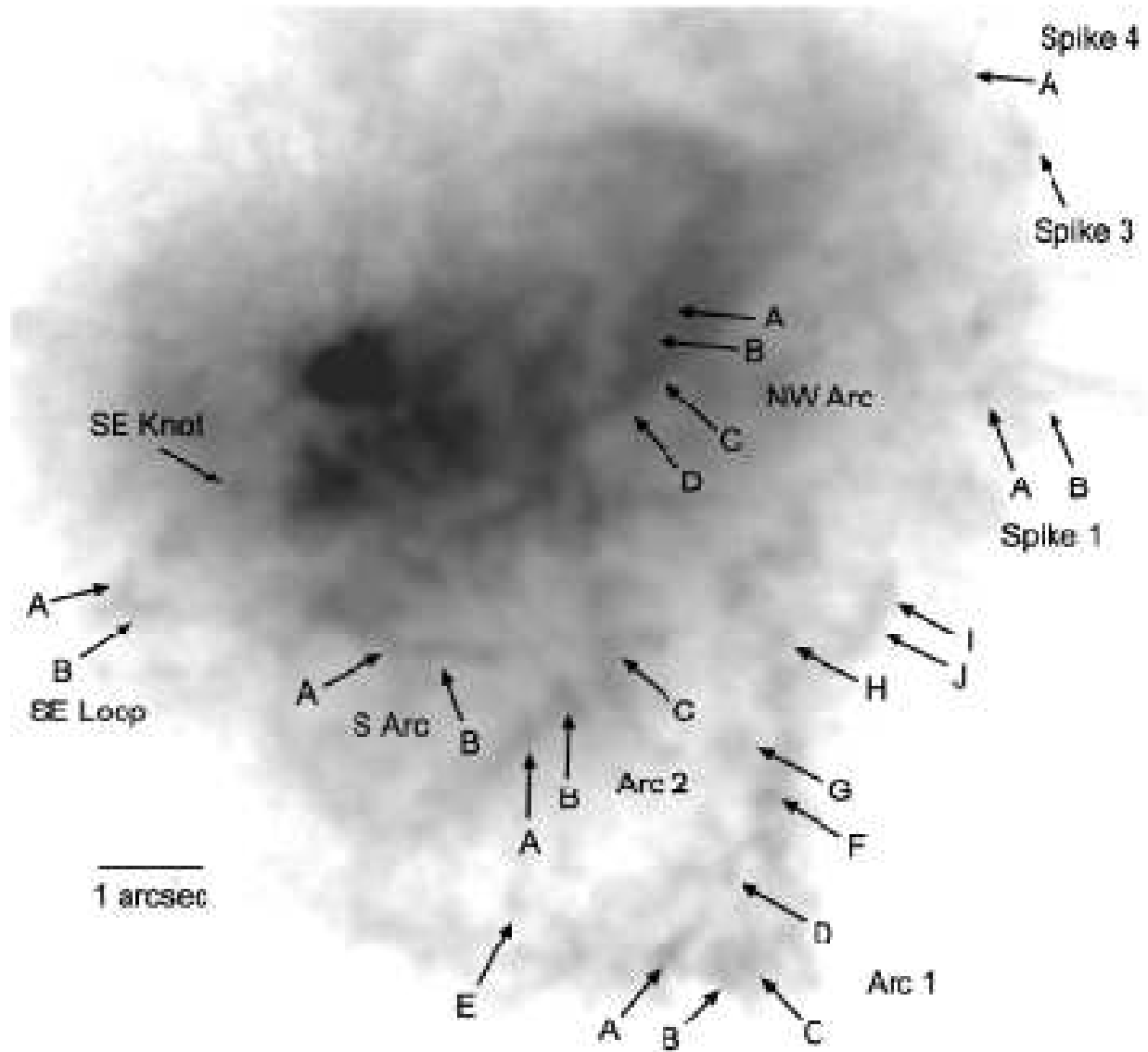


Fig. 3.— The F547M image with positions in the outer ejecta identified including Arcs 1 and 2.

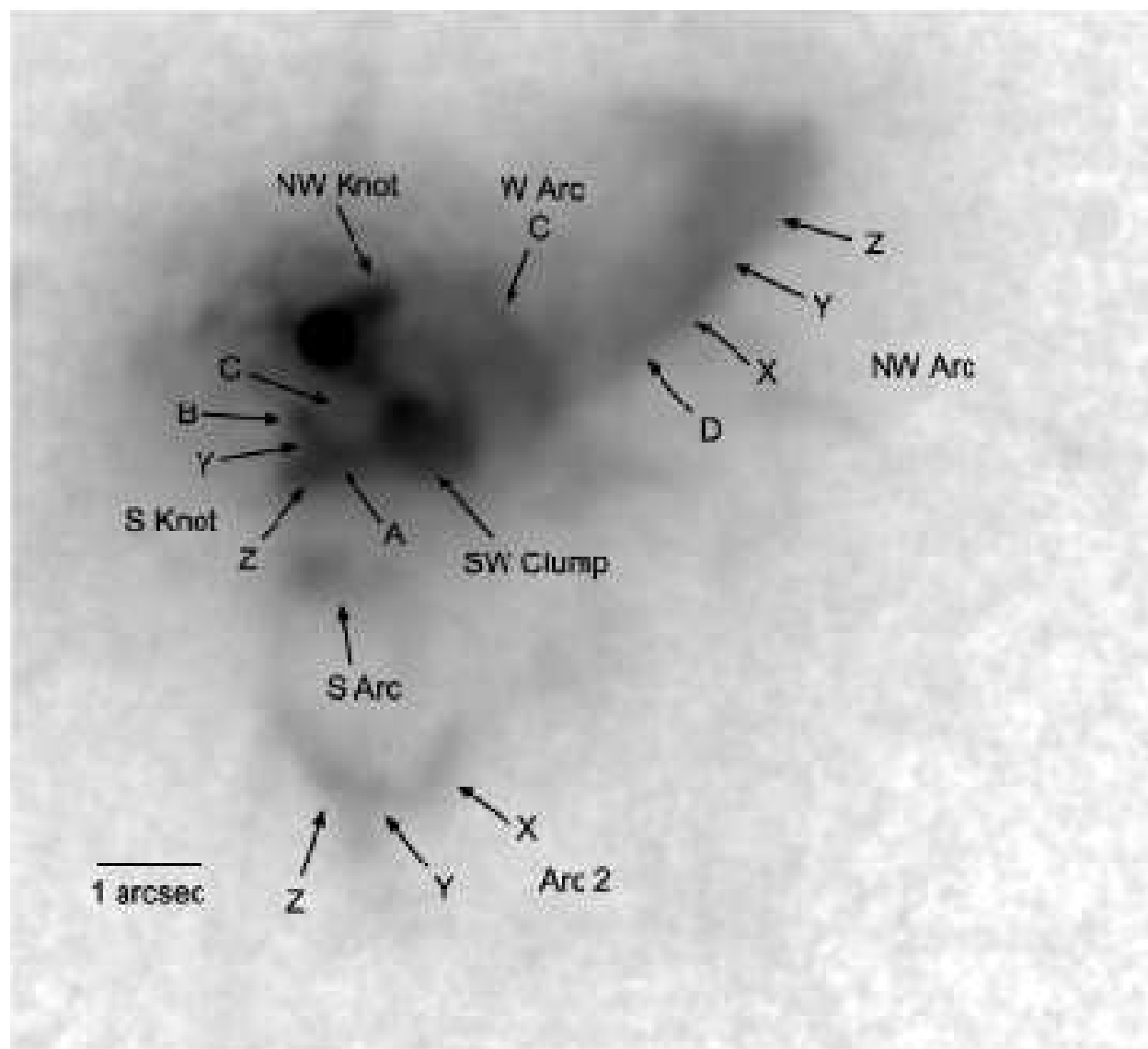


Fig. 4.— The F1042M image showing the features measured on this far-red image

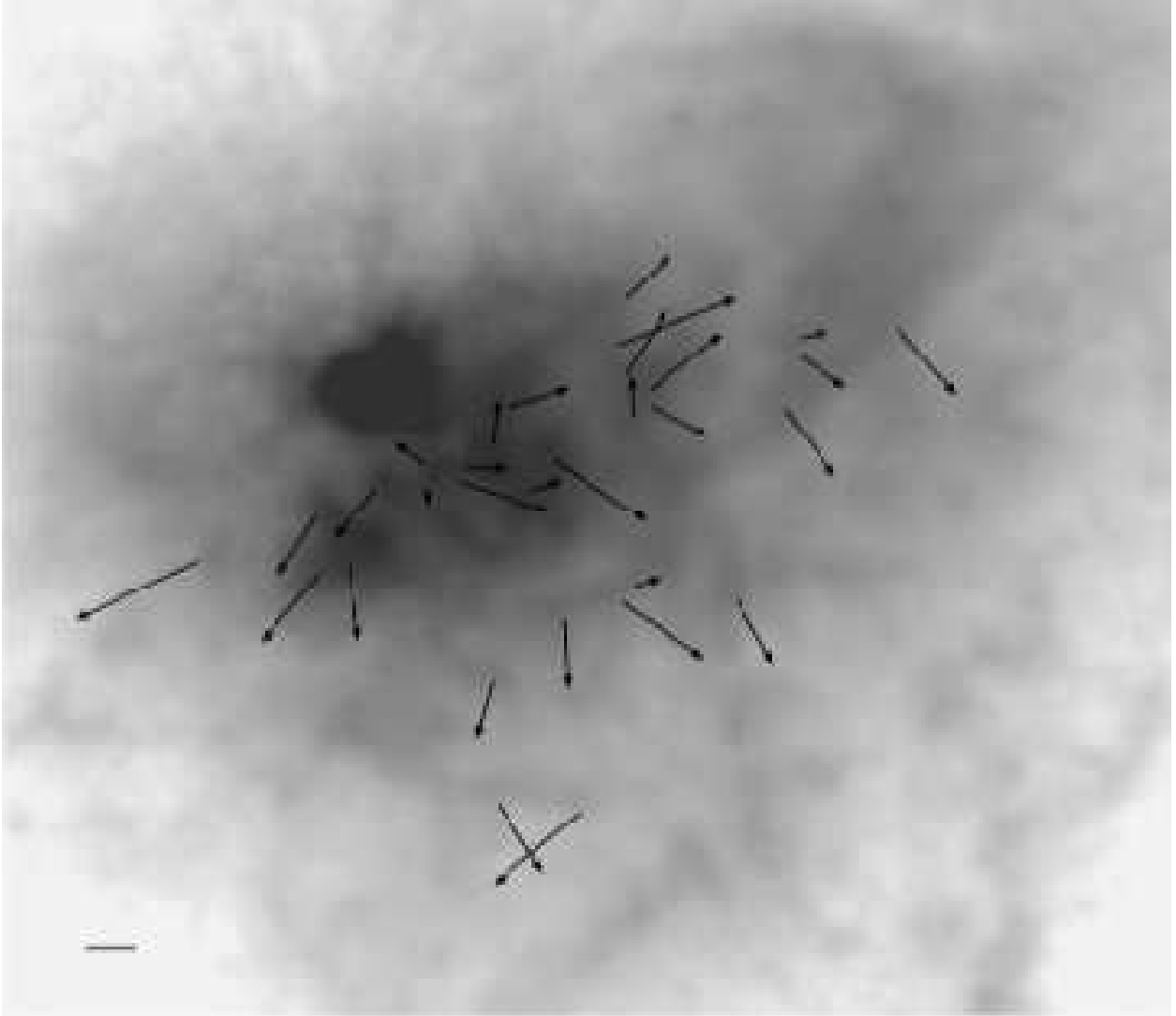


Fig. 5.— The F547M image with the velocity vectors (ϕ) for the transverse motion from Table 3. The length of the arrow is proportional to the transverse velocity; the scale bar in the lower left corner is 30 km s^{-1} . The features identified in Figures 1 and 2 are shown here.

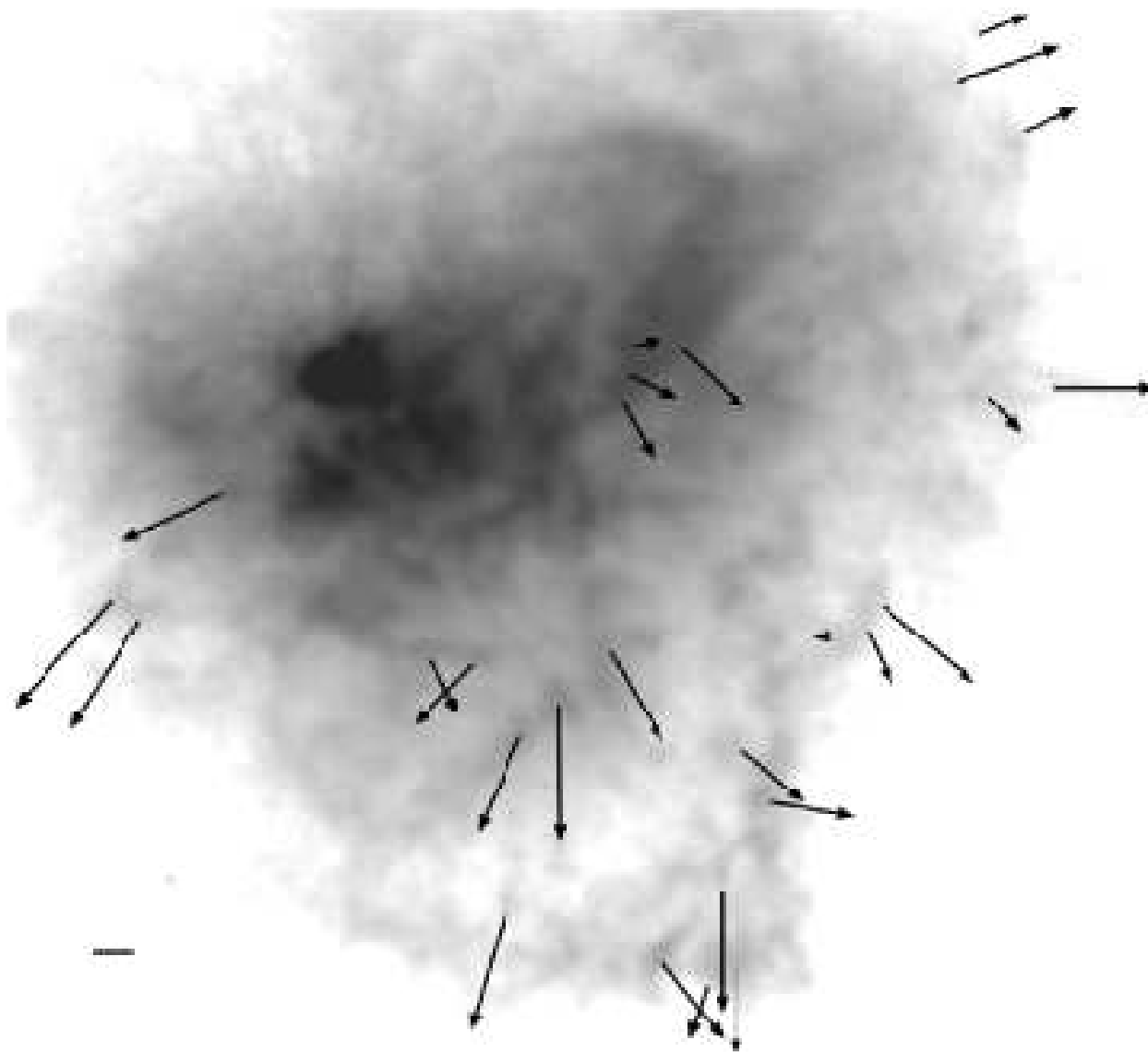


Fig. 6.— Same as Figure 5 for the features identified in Figure 3.

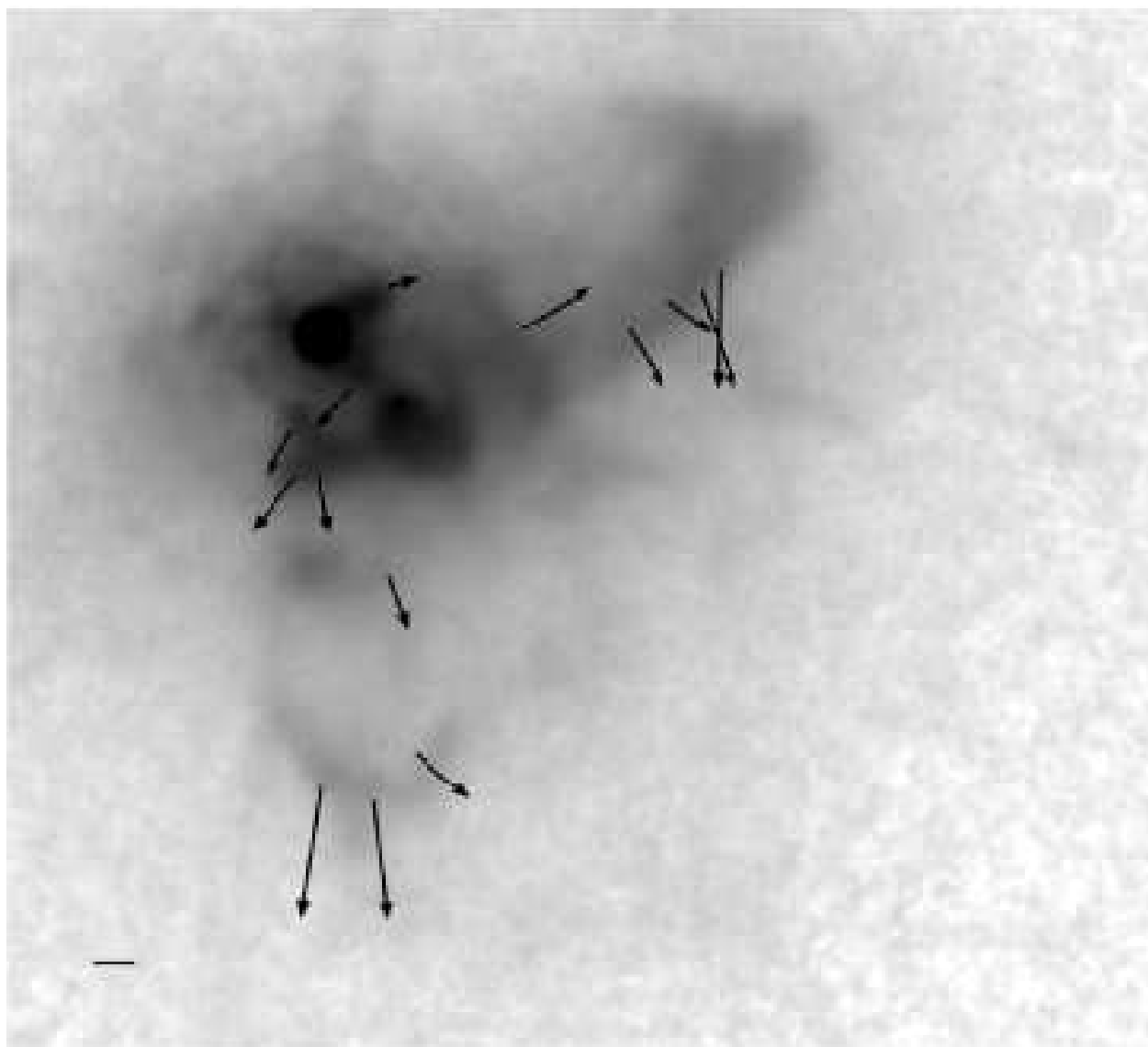


Fig. 7.— Same as Figure 5 for the features identified in Figure 4.

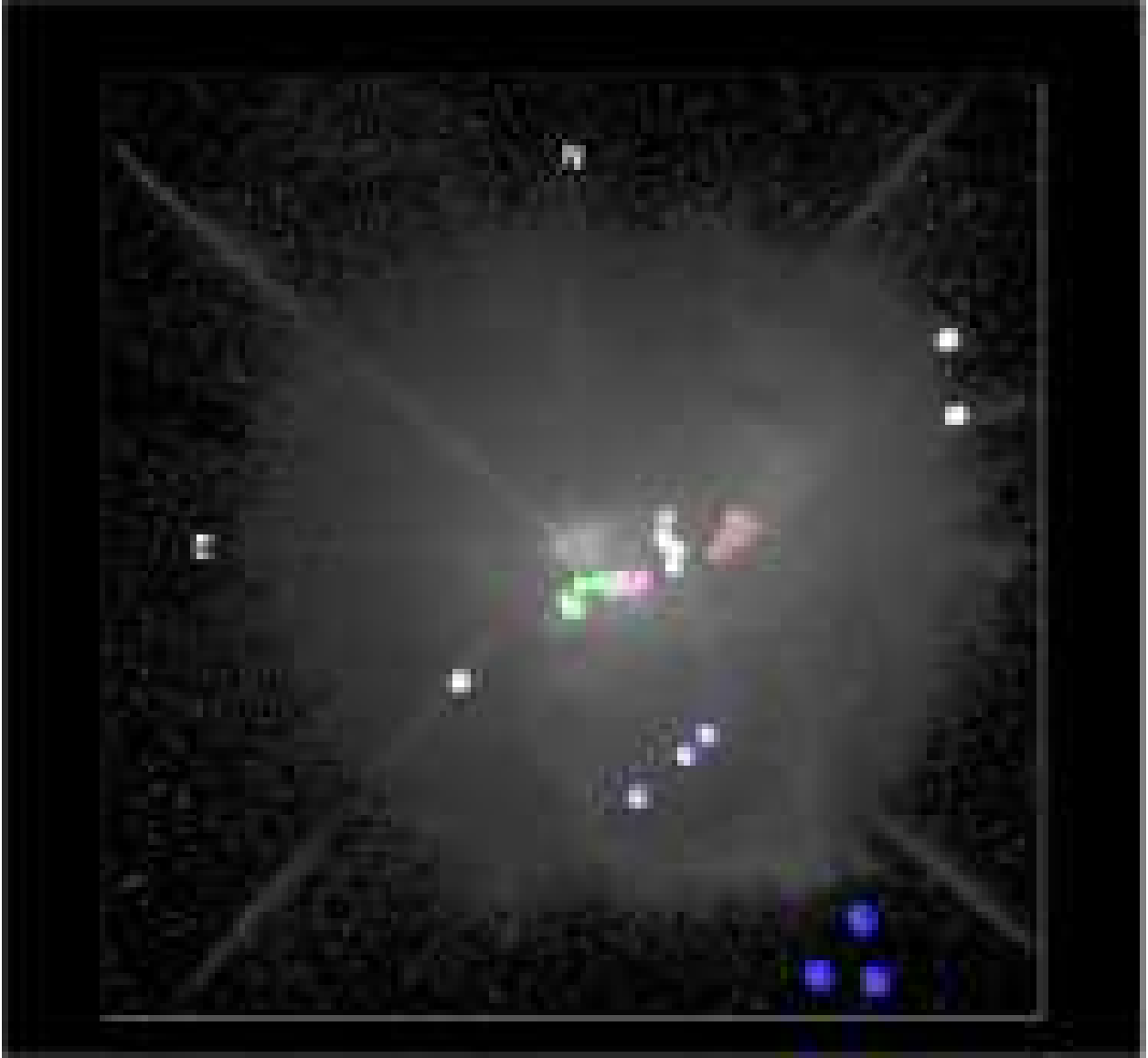


Fig. 8.— The distribution of the measured knots with total space motions and therefore positions in all three dimensions on an image of VY CMa. This is not an orthographic projection. In this projection the viewer is close to the star, hence, nearer objects (Arc 1) appear larger and at a wider angle relative to the star. The measured positions are color-coded: dark and light blue for Arcs 1 and 2, respectively, orange for the NW Arc, green for the S knots, pink for the SW knots and white for the W Arc, SE Lop, and ‘spikes’ 3 and 4.

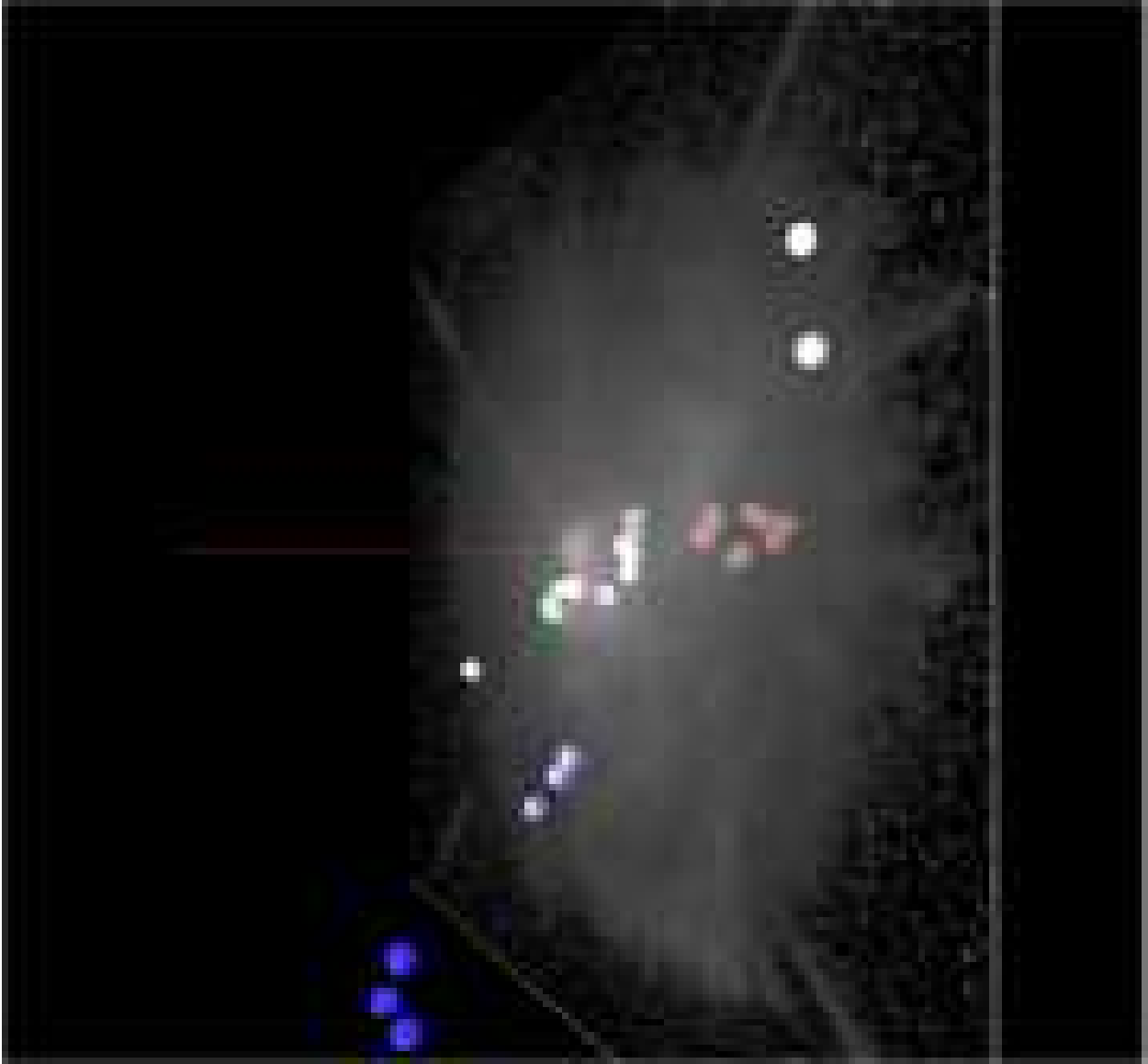


Fig. 9.— The same as Figure 8, but rotated 60° west showing the positions relative to the plane of the sky.



Fig. 10.— The same as Figure 9, but rotated 90° west or edge-on.

Table 1. Journal of New Observations

Instrument	Date	Filter	Exposure Times	Combined Images
WFPC2	June 13, 2005	F410M	5 ^s , 16 ^s , 60 ^s × 2	F410 _s (21 ^s), F410 _l (120 ^s)
		F547M	0.1 ^s , 0.5 ^s , 2 ^s , 5 ^s , 16 ^s	F547 _s (0.6 ^s), F547 _l (21 ^s)
		F656N	0.4 ^s , 2 ^s , 14 ^s , 60 ^s	F656 _s (2.4 ^s), F656 _l (74 ^s)
		F1042M	0.1 ^s , 0.5 ^s , 3 ^s , 16 ^s	F1042 _s (0.6 ^s), F1042 _l (19 ^s)
ACS/HRC	August 17, 2004	F550M/POL0V	0.2 ^s , 0.5 ^s , 5 ^s , 60 ^s	
		F550M/POL60V	”	
		F550M/POL120V	”	
		F658N/POL0V	1 ^s , 5 ^s , 40 ^s , 150 ^s	
		F658N/POL60	”	
		F658N/POL120V	”	

Table 2. Measured Angular Shifts in Arc Seconds In the Different Filter Combinations

Feature ID	F410s	F410l	F547s	F547l	F656s	F656l	F1042s	F1042l
S knot A	0.062 ± 0.004^a	0.029 ± 0.004	0.027 ± 0.002	...	0.043 ± 0.005	0.037 ± 0.004	0.008 ± 0.007^a	0.038 ± 0.005
S knot B	0.041 ± 0.001	0.029 ± 0.004	...	0.037 ± 0.004	0.048 ± 0.003^a	0.056 ± 0.003^a
S knot C	0.052 ± 0.009^a	0.015 ± 0.001	0.026 ± 0.004	...	0.019 ± 0.005	0.025 ± 0.001	...	0.065 ± 0.005^a
S knot D	0.043 ± 0.005^b	0.010 ± 0.003^c	0.034 ± 0.004^a
S knot Y	0.048 ± 0.001
SW knot A	0.067 ± 0.015^a	0.028 ± 0.002	0.012 ± 0.004	...	0.034 ± 0.004
SW knot B	0.025 ± 0.002	0.020 ± 0.003
SW knot C	0.020 ± 0.003	0.032 ± 0.003
SW knot D	0.043 ± 0.005	0.022 ± 0.002
SW knot G	...	0.017 ± 0.003	0.050 ± 0.001
SW knot H	0.035 ± 0.010
SW Clump	0.008 ± 0.002	0.025 ± 0.003
W arc A	0.062 ± 0.010^a	0.016 ± 0.006^a	0.029 ± 0.003	0.025 ± 0.003
W arc B	0.040 ± 0.001	0.025 ± 0.001^a	0.046 ± 0.003
W arc C	0.050 ± 0.004^d	0.042 ± 0.010^e	0.020 ± 0.006^a
W arc D	0.059 ± 0.005^f	0.030 ± 0.001^g
Inner W arc	0.023 ± 0.007
NW arc A	0.047 ± 0.004^h	0.044 ± 0.004^i
NW arc B	0.059 ± 0.003^j	0.039 ± 0.013^k	...	0.023 ± 0.006^l
NW arc C	0.063 ± 0.002	0.031 ± 0.002
NW arc D	0.100 ± 0.004^a	0.023 ± 0.005^m	...	0.020 ± 0.003^n
NW arc X	0.028 ± 0.004
NW arc Y	0.036 ± 0.014
NW arc Z	0.010 ± 0.010^a
NW knot	0.032 ± 0.007	0.008 ± 0.003
SE loop A	0.039 ± 0.008^o	...	0.074 ± 0.011^p
SE loop B	0.053 ± 0.004
SE knot	0.060 ± 0.006	...	0.054 ± 0.005
Inner S arc A	0.036 ± 0.014	...	0.018 ± 0.005
Inner S arc B	0.040 ± 0.001
S arc A	0.040 ± 0.015	...	0.034 ± 0.002
S arc B	0.038 ± 0.011	...	0.044 ± 0.002
SW arc A	0.036 ± 0.011
SW arc B	0.042 ± 0.002	...	0.015 ± 0.005
SW arc C	0.011 ± 0.004

Table 2—Continued

Feature ID	F410s	F410l	F547s	F547l	F656s	F656l	F1042s	F1042l
Finger	0.053 ± 0.009	...	0.031 ± 0.004
Arc 2 A	0.059 ± 0.002	...	0.036 ± 0.003
Arc 2 B	0.059 ± 0.003	...	0.034 ± 0.008
Arc 2 C	0.039 ± 0.005
Arc 2 X	0.048 ± 0.001
Arc 2 Y	0.071 ± 0.005
Arc 2 Z	0.075 ± 0.022
Arc 1 A	0.053 ± 0.006	...	0.037 ± 0.003
Arc 1 B	0.050 ± 0.001 ^a	...	0.069 ± 0.003 ^f
Arc 1 C	0.047 ± 0.007
Arc 1 D	0.053 ± 0.005	...	0.066 ± 0.010
Arc 1 E	0.058 ± 0.002
Arc 1 F	0.042 ± 0.005	...	0.062 ± 0.001
Arc 1 G	0.022 ± 0.004 ^g	...	0.073 ± 0.016 ^t
Arc 1 H	0.006 ± 0.006 ^a
Arc 1 I	0.056 ± 0.004
Arc 1 J	0.019 ± 0.003
Spike 1 A	0.025 ± 0.006
Spike 1 B	0.086 ± 0.005
Spike 3 A	0.035 ± 0.005
Spike 4 A	0.064 ± 0.009
Spike 4 B	0.024 ± 0.010

^aDiscrepant positions, not used.

^bS knot D1

^cS knot D2

^dW arc C1

^eW arc C2

^fW arc D1

^gW arc D2

^hNW arc A1

ⁱNW arc A2
^jNW arc B1
^kNW arc B2
^lNW arc B3
^mNW arc D1
ⁿNW arc D2
^oSE loop A1
^pSE loop A2
^qArc 1 B1
^rArc 1 B2
^sArc 1 G1
^tArc 1 G2

Table 3. The Transverse Velocities, Direction of Motion and Positions

Feature Id	Radial Distance from Star (arcsec)	Position Angle from Star (deg)	Weighted Mean Transverse Velocity V_T (km s ⁻¹)	Direction of Motion (ϕ) (deg)
S knot A	0.97	-176	36.7 ± 2.4	177 ± 5
S knot B	0.85	176	37.7 ± 2.5	148 ± 7
S knot C	0.63	-163	22.8 ± 1.0	151 ± 12
S knot D1	0.73	-140	49.4 ± 6.9	46 ± 4
S knot D2	0.85	-131	11.4 ± 4.3	21 ± 17
S knot Y	0.98	179	55 ± 2	147 ± 2
SW knot A	0.99	-121	30.2 ± 2.5	-101 ± 23
SW knot B	1.01	-120	27.3 ± 2.6	-3 ± 9
SW knot C	1.18	-121	29.9 ± 3.1	-95 ± 30
SW knot D	0.83	-100	29.4 ± 3.3	-63 ± 11
SW knot G1	1.23	-115	19.2 ± 4.5	-50 ± 12
SW knot G2	1.23	-115	57.6 ± 1.3	-119 ± 4
SW knot H	0.84	-99	40.6 ± 15.1	-104 ± 8
SW Clump	0.97	-135	17.7 ± 2.5	-162 ± 15
W arc A	1.71	-92	30.5 ± 2.7	-72 ± 30
W arc B	1.69	-100	48.4 ± 2.0	-24 ± 23
W arc C1	1.56	-87	57.0 ± 5.0	-57 ± 3
W arc C2	1.70	-91	48.2 ± 13.5	-57 ± 5
W arc D1	1.50	-82	67.5 ± 7.8	-69 ± 2
W arc D2	1.64	-72	34.1 ± 2.5	-40 ± 2
Inner W arc	1.69	-90	26.3 ± 9.5	-139 ± 3
NW arc A1	3.14	-82	53.9 ± 6.0	-122 ± 2
NW arc A2	2.92	-79	50.1 ± 5.2	-145 ± 1
NW arc B1	2.85	-82	68.8 ± 3.5	-87 ± 2
NW arc B2	2.66	-85	44.8 ± 19	-120 ± 23
NW arc B3	2.91	-80	26.8 ± 8.3	-27 ± 8
NW arc C	2.63	-86	52.0 ± 1.8	-88 ± 19
NW arc D1	2.57	-92	26.8 ± 7.4	-156 ± 11
NW arc D2	2.69	-90	23.5 ± 4.9	-21 ± 4
NW arc X	3.04	-87	32.5 ± 5.8	-107 ± 7
NW arc Y	3.26	-83	41.7 ± 16	-110 ± 8
NW knot	0.46	-58	14.6 ± 4.2	-78 ± 5
SE loop A1	2.68	137	44.9 ± 12	105 ± 12
SE loop A2	2.72	140	85.2 ± 15.6	133 ± 7
SE loop B	2.67	140	60.7 ± 6.4	161 ± 9
SE knot	1.33	141	64.5 ± 5.9	124 ± 11
Inner S arc A	1.92	-155	23.6 ± 6.8	165 ± 8
Inner S arc B	1.59	-162	48.1 ± 2.6	130 ± 3
S arc A	2.82	-152	50.0 ± 2.8	-163 ± 11
S arc B	2.63	-159	39.1 ± 2.5	152 ± 11
SW arc A	1.80	-138	41.6 ± 9.7	-175 ± 3
SW arc B	1.97	-129	40.0 ± 3.3	-151 ± 13
SW arc C	1.82	-139	13.2 ± 6.1	-66 ± 11
Finger	2.56	-117	39.6 ± 4.9	-150 ± 4

Table 3—Continued

Feature Id	Radial Distance from Star (arcsec)	Position Angle from Star (deg)	Weighted Mean Transverse Velocity V_T (km s ⁻¹)	Direction of Motion (ϕ) (deg)
Arc 2 A	3.59	-151	63.1 ± 2.0	155 ± 7.5
Arc 2 B	3.50	-144	64.2 ± 3.7	-170 ± 15
Arc 2 C	3.41	-135	44.6 ± 6.8	-146 ± 5
Arc 2 X	3.91	-165	55.9 ± 2.0	-135 ± 2
Arc 2 Y	4.09	-175	81.5 ± 6.5	-171 ± 8
Arc 2 Z	3.92	-179	85.9 ± 26	174 ± 5
Arc 1 A	5.89	-150	52.7 ± 3.0	-138 ± 5
Arc 1 B1	6.28	-147	56.9 ± 2.1	126 ± 6
Arc 1 B2	6.35	-147	88.1 ± 15.2	-109 ± 1
Arc 1 C	6.31	-145	54.4 ± 10.0	180 ± 2
Arc 1 D	5.61	-142	64.3 ± 6.8	-175 ± 4
Arc 1 E	4.92	-161	67.1 ± 3.0	161 ± 4
Arc 1 F	5.33	-134	69.8 ± 1.8	-113 ± 25
Arc 1 G1	4.85	-132	25.6 ± 6.2	-177 ± 20
Arc 1 G2	4.75	-134	84.1 ± 22.4	-121 ± 2
Arc 1 I	5.17	-111	64.4 ± 5.6	128 ± 5
Arc 1 J	5.21	-115	22.3 ± 5.4	-158 ± 16
Spike 1A	5.72	-92	28.9 ± 8.1	-138 ± 11
Spike 1B	6.61	-91	98.2 ± 6.9	-92 ± 3
Spike 3	6.40	-71	40.5 ± 6.9	-76 ± 11
Spike 4A	6.05	-65	73.5 ± 13.1	-75 ± 4
Spike 4B	6.76	-61	27.8 ± 14.2	-75 ± 6

Table 4. Summary of the Motions in the Circumstellar Ejecta

Feature Id	V_x (km s ⁻¹)	V_y (km s ⁻¹)	ϕ (deg)	V_z (km s ⁻¹)	θ (deg)	V_{Tot} (km s ⁻¹)	Comment
S knot A	1.9	-36.6	177	-17	-24.8	40.4	Slit V ap 3
S knot B	20	-32	148	-17	-24.3	41.3	Slit V ap 3
S knot C	11	-19.9	151	-15	-33.3	27.3	between III Ap 1 and 2 ^a
S knot D1	35.5	34.3	46	-14	-15.8	51.3	Slit III ap 2
S knot D2	4.1	10.6	21	-14	-50.8	18.0	Slit III ap 2
S knot Y	30	-46	147	-16	-16	57.3	Slit V ap 3
SW knot A	-29.6	-5.8	-101	-14	-24.9	33.3	Slit III ap 2
SW knot B	-1.4	27.3	-3	-14	-27.1	30.7	Slit III ap 2
SW knot C	-29.8	-0.1	-95	-14	-25.1	33.0	Slit III ap 2
SW knot G1	-14.7	12.3	-50	-14	-36	23.8	Slit III ap 2
SW knot G2	-50.4	-27.9	-119	-14	-13.7	59.3	Slit III ap 2
SW Clump	-5.5	-16.8	-162	2.5:	8:	17.8	Slits III ap 2 and II ap 3
W arc A	-29	9.4	-72	0	0	30.5	Slit III ap 3
W arc B	-19.7	44.2	-24	0	0	30.5	Slit III ap 3
W arc C1	-47.8	31	-57	0	0	57	Slit III ap 3
W arc C2	-40.4	26.2	-57	0	0	48.2	Slit III ap 3
W arc D1	-63	24.2	-69	4	9.7	67.6	Slit I ap 3
W arc D2	-21.8	26.0	-40	4	6.7	34.2	Slit I ap 3
NW arc A1	-45.7	-28.6	-122	19	19.4	57.1	Slit III ap 4
NW arc A2	-28.7	-41.0	-145	19	20.8	53.6	Slit III ap 4
NW arc B1	-68.7	3.6	-87	9	7.5	69	between III ap 3 and 4 ^b
NW arc B2	-38.8	-22.4	-120	9	11.3	45.7	between III ap 3 and 4 ^b
NW arc B3	-12.2	23.9	-27	9	18.6	28.3	between III ap 3 and 4 ^b
NW arc C	-51.9	1.8	-88	9	9.8	52.8	between III ap 3 and 4 ^b
NW arc D1	-10.9	-24.5	-156	18.7	35	32.7	Slit II ap 5
NW arc D2	-8.4	21.9	-21	18.7	38.5	30.0	Slit II ap 5
NW arc X	-31.1	-9.5	-107	23	35.3	39.8	between II ap 5 and 6 ^c
NW arc Y	-39.2	-14.2	-110	23	28.9	47.6	between II ap 5 and 6 ^c
NW knot ^d	-14.3	3.0	-78	
SE Loop B	19.8	-57.4	161	-23.5	-21	65.1	Slit III, new position
Inner S arc A	6.1	-22.8	165	-13	-28.8	26.9	Slit V ap 4
S arc B	18.4	-34.5	152	-16	-22.2	42.2	between V ap 4 and 5 ^e
Arc 2 A	26.7	-57.2	155	-19	-16.7	65.9	Slit V ap 5
Arc 2 B	-11.1	-63.2	-170	-19	-16.5	67	Slit V ap 5
Arc 2 X	-39.5	-39.5	-135	-19	-18.8	59.0	Slit V ap 5
Arc 1 A	-35.2	-39.1	-138	-37	-35	64.4	Slit V ap 7
Arc 1 C	-54.5	-37	180	-37	-34	65.9	Slit V ap 7
Arc 1 D	-5.6	-64.0	-175	-37	-29.9	74.2	Slit V ap 7
Spike 3	-39.3	9.8	-76	-6 or 0	-8.4 or 0	40.5	Slit II ap 8 ^f
Spike 4B	-26.8	7.2	-75	-6 or 0	-12 or 0	28.4	slit I ap 6

^aVelocity interpolated between apertures 1 and 2.

^bVelocity interpolated between apertures 3 and 4.

^cVelocity interpolated between apertures 5 and 6.

^dSame aperture as star.

^eVelocity interpolated between apertures 4 and 5

^fTwo velocities are measured at 35 and 41 km s⁻¹. It is not possible to tell which is the appropriate velocity for this feature, but it makes little difference for the result.

Table 5. Summary of Vector Motions and Ejection Ages for the Major Features

Feature	V_{Tot} (km s ⁻¹)	θ (deg)	Mean ϕ^a (deg)	Ejection Age (years)
NW Arc	45.7 ± 4	22 ± 7	-98 ± 13^b	500 ± 50
Arc 1	68.2 ± 2.5	-33 ± 3	-161 ± 13^c	800 ± 50
Arc 2	64 ± 2.1	-17 ± 1	-174 ± 8^d	400 ± 15
W Arc	43.7 ± 4.8	$\sim 0 \pm 3$	-53 ± 7	300 ± 30
SW Knots	36 ± 5.5	-25 ± 3	-86 ± 14^e	250 ± 50
S Knots	41.6 ± 5	-27 ± 4	156 ± 6^f	157 ± 25
S Arc ^g	42.2 ± 2.5	-22	174 ± 8	480 ± 25
SE Loop	65.1 ± 4.6	-21	133 ± 13	320 ± 20
SW Clump	~ 18	8:	-162	500
“spikes”	30 – 40	~ 0	... ^h	1300 – 1700

^aMean position angle of the tranverse motions (Table 3)

^bWith a lack of measurements at the tip and in the hook of the NW Arc, this result is uncertain.

^cArc1 excluding knots I and J.

^dArc 2 excluding knot C.

^eExcluding knot B, but the SW Knots may be expanding away from each other.

^fS Knots excluding D1 and D2.

^gknot B only; an alternate choice of Doppler velocity gives a vector direction away from us at +16°, but the same ejection age.

^hSpikes 3 and 4 have the same ϕ of -75°.